Energy-Optimized Path Planning for Autonomous Ferries

Glenn Bitar * **Morten Breivik** * **Anastasios M. Lekkas** *

* *Centre for Autonomous Marine Operations and Systems, Department of Engineering Cybernetics, Norwegian University of Science and Technology (NTNU), NO-7491 Trondheim, Norway. E-mail: {glenn.bitar,anastasios.lekkas}@ntnu.no, morten.breivik@ieee.org*

Abstract: The topic of energy-optimized path planning using pseudospectral optimal control is considered. An optimal control problem (OCP) is formulated to produce an energy-optimized path between two points among static obstacles. A nonlinear 3-degree-of-freedom underactuated ship model is considered in the OCP with an energy-based cost function. The ship model is affected by external disturbances in the form of ocean currents. The OCP is solved using a pseudospectral method, which has proven successful in real-world applications. Additionally, the method is not as sensitive to dimensionality compared to Hamilton-Jacobi-Bellman methods. Position and speed information from the OCP solution is used in a closed-loop simulation with a guidance controller to show feasibility of the path. The simulation results show that the path is feasible, and that including ocean-current information in the path planning significantly reduces energy consumption. The paper also gives a short overview and classification of alternative path-planning methods. Finally, a proposal for how the path planner fits in a complete motion-control architecture is provided.

Keywords: Path planning, energy optimization, autonomous ships, optimal control

1. INTRODUCTION

Being a coastal country with a large prevalence of mountains and fjords, transportation has always been a challenge in Norway. Ferries are commonly used across large bodies of water, where construction of bridges is not cost effective or even possible. In 2017, Norway had around 150 ferry connections, where most of these are marked in Fig. 1. Approximately 9 % of the Norwegian domestic CO_2 emissions are caused by ships, where a significant portion is caused by passenger ships (DNV GL, 2014). As the focus on emission-free transportation increases, so does the need for energy-efficient solutions. Battery-powered ferries are low-emission solutions tested in Norwegian waters, and will be an important factor towards emission-free transportation, since the country's goal is to have a zero-emission maritime industry by 2050 (Criscione, 2017). However, battery-powered vessels are more limited in range than those powered by fossil fuel. This is due to challenges related to cost and weight of the energy storage (Kongsberg Maritime et al., 2017). Optimizing motion control may increase the operation envelope for battery solutions. Increasing the autonomy level of motion control systems will to a greater extent facilitate energy optimization. Rolls-Royce are among the industrial initiators for autonomy in ferries with their "Auto-Crossing" system, aimed to make energy consumption predictable (Rolls-Royce, 2016). Furthermore, the work presented in this paper is part of another industrial initiative for energy-optimized autonomous ferries, with project partners Kongsberg Maritime, Fjellstrand, Grenland Energy,

Fig. 1. Overview of Norwegian ferry connections.

Grønn Kontakt and NTNU in a Pilot-E funded initiative (Kongsberg Maritime et al., 2017).

This work presents a method for performing energy-optimized path planning using pseudospectral (PS) optimal control. A nonlinear, underactuated 3-degree-of-freedom (DOF) ship model affected by external disturbances in the form of ocean currents is used in both planning and simulation. The planner finds an optimized path using an energy-based cost function, which is then used by a guidance controller. The optimization is performed on

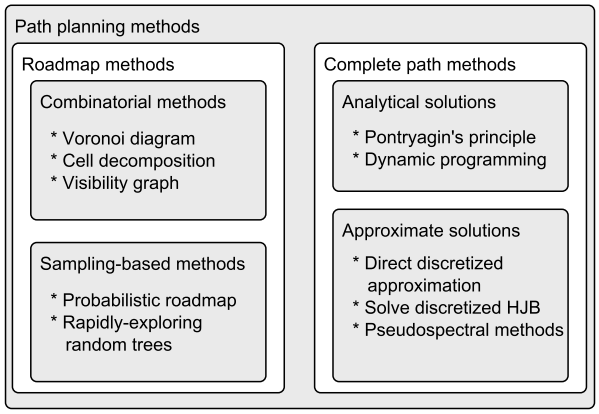

Fig. 2. Hierarchy of path-planning methods.

the three pose states, namely north and east position and heading, and on three velocity states, namely surge, sway and yaw rate. The work is a continuation of the master's thesis (Bitar, 2017), where several aspects of autonomy in ferries are considered, including path-planning methods, collision avoidance (COLAV), automatic docking and industrial control systems. Although the method presented in this work is designed for use with ferries, it can also be applied to other underactuated ships. The purpose of this paper is a show of concept, and not an extensive study of the method, therefore aspects such as failure handling, actuator limitations and state estimation are not considered.

Extensive research has been performed on path planning and motion planning in robotics literature. Useful references include (Wolek and Woolsey, 2017), where several model-based methods are reviewed. These methods include optimal control, level set methods, roadmap methods and others which are suitable for marine vehicles. Two distinct categories of path-planning methods are *roadmap methods* and *complete path methods*. Roadmap methods produce waypoints which form a feasible path if connected. Complete path methods generate a continuous parametrized path, often by optimization or optimal control. Figure 2 classifies some of the most important path-planning methods in a hierarchical manner.

Roadmap methods may be further divided by computational complexity. The two main subcategories are *combinatorial* and *sampling-based* methods. Combinatorial planning is also called exact planning, and considers the whole continuous space for roadmap vertices, which is inherently computationally expensive. Sampling-based methods are probabilistic and consider only an amount of sampled points in the continuous space, and thus have shorter running times for high-dimensional problems.

Optimization-based complete path methods are usually based on optimal control. A state-trajectory is found by using a solver, e.g. dynamic programming, which involves solving the Hamilton-Jacobi-Bellman (HJB) partial differential equation (PDE), or by using a pseudospectral algorithm, which is the solution presented in this paper. Other optimization-based methods include e.g. model predictive control (MPC).

Several researchers demonstrate the use of pseudospectral methods for motion planning and path planning. Lekkas et al. (2016) use pseudospectral optimal control to perform time-optimized path planning for a 3-DOF ship model. Re-planning at set intervals is also performed, such that updated estimates of environmental forces are taken into account. However, the authors use a reduced-order model, assume zero sideslip, while yaw-rate is treated as an input. Gong et al. (2009) perform motion planning on several kinds of vehicles using pseudospectral optimal control. These experiments involve complex environments and models, but no guidance simulations with disturbances are performed. Ross and Karpenko (2012) mention several successful demonstrations of the use of pseudospectral methods, among them a minimum-time rotational maneuver of a space telescope in orbit, and a zero-propellant maneuver of the International Space Station.

The main contribution of this paper is a method for performing model-based energy-optimized path planning using pseudospectral optimal control with an energy-based cost function. While pseudospectral optimal control has been used to generate motion trajectories in other references, the use of an energy-based cost function to create the path is novel. Path feasibility is shown by performing simulations with a curved-path guidance algorithm. The simulations indicate that energy can indeed be saved by performing path planning with up-to-date ocean current information.

The paper is organized as follows: Section 2 proposes a control system architecture for transit operations, including blocks for path planning, guidance, COLAV, low-level control and sensors; Section 3 treats ship modeling and control; Section 4 introduces the optimization-based path planning method; Section 5 discusses the planning and simulation results, while Section 6 concludes the paper.

2. MOTION CONTROL ARCHITECTURE

Motion control in ferry operations consist of undocking, a controlled maneuver away from the dock area, transit towards the destination dock, and docking. A proposed control system architecture for transit is illustrated in Fig. 3, where the highlighted block is the path planner which is the focus of this paper. Other important blocks are the mid-level and reactive COLAV subsystems, as defined by Eriksen and Breivik (2017).

COLAV is the task of avoiding collisions with static and moving obstacles. The task may be split into three levels: High-level global path planning, mid-level protocol-based COLAV, and low-level reactive COLAV. Low-level COLAV is responsible for avoiding immediate collision, and does not care about e.g. the International Regulations for Preventing Collisions at Sea (COLREG). Mid-level COLAV is intended to prevent collisions by following a set of rules, e.g. the COLREG. Methods at this level should also perform distinct maneuvers that communicate intended actions to onlookers and other vessels. High-level planning is responsible for creating paths that avoid known static obstacles such as land and reefs.

The low-level and mid-level methods rely upon local sensor information about dynamic and static obstacles. Target

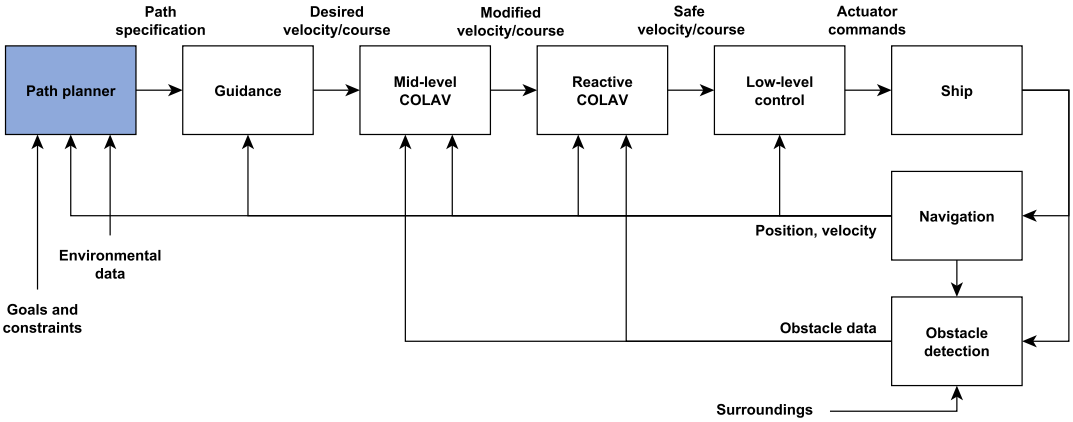

Fig. 3. Block diagram of motion control architecture during transit.

tracking and related sensory technology are key to retrieving this information. Wilthil et al. (2017) present a method for tracking targets with radar based on the probabilistic data association filter (PDAF). More references to target tracking methods are found therein. Eriksen and Breivik (2017) use nonlinear MPC to perform mid-level COLAV which is partly COLREG compliant. A cost function penalizing gentle turns and small speed changes is implemented to conform to the COLREG rule 8, which states that "action taken to avoid collision should be positive, obvious and made in good time." The high-level planner relies on static information about the area, such as a map. Various techniques may be implemented to provide a two-dimensional feasible path for the ship to follow using a guidance system. One such technique is explored in Section 4.

3. SHIP MODELING AND CONTROL

3.1 Modeling

We use an underactuated 3-DOF nonlinear ship model for path planning and simulation. The modeling techniques and notation are retrieved from (Fossen, 2011). The ship is called Cybership II, and is a 1:70 scale replica of a supply ship, with a length of $L = 1.255\,\text{m}$ and mass $m = 23.8\,\text{kg}$. Information about this model ship and its physical parameters is found in (Skjetne et al., 2005). To scale velocities and other variables up to its full-scale equivalent, one may use the bis scaling system, described in e.g. (Fossen, 2011). The scaling factor for linear velocities for this ship is $\sqrt{\frac{L_f}{L}}$, where L_f is the length of the full-scale ship, resulting in a factor of $\sqrt{70}$. The model is written on the following form, with the time dependency omitted for notational brevity:

$$\dot{\boldsymbol{\eta}} = \mathbf{R}(\psi)\boldsymbol{\nu} \tag{1a}$$

$$\mathbf{M}\dot{\boldsymbol{\nu}}_r + \mathbf{C}(\boldsymbol{\nu}_r)\boldsymbol{\nu}_r + \mathbf{D}(\boldsymbol{\nu}_r)\boldsymbol{\nu}_r = \boldsymbol{\tau}. \tag{1b}$$

Here $\boldsymbol{\eta} = [x, y, \psi]^\top$ is the ship's pose, where x and y are the north and east position, respectively, and ψ is the ship's heading. The rotation matrix $\mathbf{R}(\psi)$ is defined as

$$\mathbf{R}(\psi) = \begin{bmatrix} \cos\psi & -\sin\psi & 0 \\ \sin\psi & \cos\psi & 0 \\ 0 & 0 & 1 \end{bmatrix}. \tag{2}$$

The ship's velocity over ground in BODY coordinates $\{b\}$ is $\boldsymbol{\nu} = [u, v, r]^\top$, where u is surge speed, v is sway speed, and r is the yaw rate. The ship's velocity relative to water is used to model currents: $\boldsymbol{\nu}_r = [u_r, v_r, r]^\top = \boldsymbol{\nu} - \boldsymbol{\nu}_c$. We have denoted the current velocity in BODY as $\boldsymbol{\nu}_c = [u_c, v_c, 0]^\top$. The current velocity in NED coordinates $\{n\}$ is $\boldsymbol{\nu}_c^n = [V_x, V_y, 0]^\top$, and the relationship between those is $\boldsymbol{\nu}_c = \mathbf{R}^\top(\psi)\boldsymbol{\nu}_c^n$.

In (1), $\mathbf{M} \in \mathbb{R}^{3\times3}$ is the symmetric, positive definite system inertia matrix. We denote the Coriolis and centripetal matrix $\mathbf{C}(\boldsymbol{\nu}_r) \in \mathbb{R}^{3\times3}$, and the damping matrix $\mathbf{D}(\boldsymbol{\nu}_r) \in \mathbb{R}^{3\times3}$. The vector $\boldsymbol{\tau} = [X, Y, N]^\top$ contains the control forces. We use an actuator model with two input signals $\boldsymbol{u} = [F, \delta]^\top$, where F is the force produced by a rear-mounted azimuth thruster, and δ is its angle:

$$\boldsymbol{\tau}(\boldsymbol{u}) = \left[F\cos\delta,\ 0,\ -l_{th}F\sin\delta\right]^\top, \tag{3}$$

where l_{th} is the length from the BODY origin to the azimuth thruster. The second element $\tau_2 = Y$ is set to zero, because it is possible to do a coordinate transformation on any ship model to achieve this property (Fredriksen and Pettersen, 2004).

3.2 Guidance controller

The guidance controller used in simulation is a curved-path line-of-sight (LOS) controller developed by Breivik and Fossen (2004). The key geometric variables are illustrated in Fig. 4. The particle $\boldsymbol{p}_d(\theta)$ is the origin of the path-parallel frame $\{p\}$. This particle exists on the path $\mathcal{P} = \{\boldsymbol{p} \in \mathbb{R}^2 | \boldsymbol{p} = \boldsymbol{p}_d(\theta)\,\forall\,\theta \in [0, \theta_{\max}]\}$. The path variable θ is interpreted as some distance along the path, and is the time variable from the path planner, as discussed in Section 4. The along-track error $s(t)$ is the tangential distance from the path particle, whereas $e(t)$ is the cross-track error. The relationship between the ship's position $\boldsymbol{p}(t) = [x(t), y(t)]^\top$ and the error variables is

$$\boldsymbol{\varepsilon}(t) = \left[s(t),\ e(t)\right]^\top = \mathbf{R}_t^\top(\chi_t(\theta))(\boldsymbol{p}(t) - \boldsymbol{p}_d(\theta)), \tag{4}$$

where $\mathbf{R}_t \in \mathbb{R}^{2\times2}$ is equivalent to the upper-left block in (2).

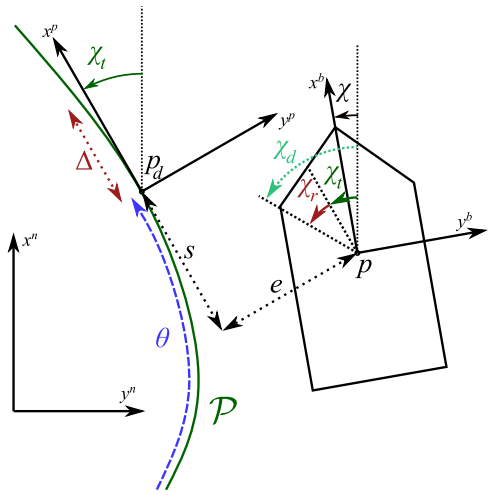

Fig. 4. Geometric variables used in guidance.

The path-tangential angle is $\chi_t(\theta)$, and the ship's course is $\chi(t)$. A control law is applied to drive $e(t)$ asymptotically to 0: $\chi_d(t) = \chi_t(\theta) + \chi_r(t)$, where $\chi_d(t)$ is the desired course angle, and $\chi_r(t) = \arctan\left(-\frac{e(t)}{\Delta}\right)$. The tuning parameter $\Delta > 0$ may be interpreted as the ship's lookahead distance. Finally, dynamics are added to the path parameter to drive it forwards:

$$\dot{\theta} = \frac{U(t)\cos(\chi(t) - \chi_t(\theta)) + \gamma s(t)}{\sqrt{x_d'(\theta)^2 + y_d'(\theta)^2}}, \tag{5}$$

where $U(t) = \sqrt{u(t)^2 + v(t)^2}$ and $\gamma > 0$ is a tuning parameter deciding the particle's convergence speed to the ship's position. Prime notation for derivatives is used: $x_d'(\theta) = \frac{\mathrm{d}x_d}{\mathrm{d}\theta}(\theta)$.

3.3 Surge and heading controller

The low-level controller is also retrieved from Breivik and Fossen (2004). A short summary of the control law follows:

$$\boldsymbol{\tau} = \mathbf{M}\dot{\boldsymbol{\alpha}} + \mathbf{N}(\boldsymbol{\nu})\boldsymbol{\alpha} - \mathbf{R}(\psi)^\top \hat{\boldsymbol{b}} - \boldsymbol{h}z_1 - \mathbf{K}_2\boldsymbol{z}_2, \tag{6}$$

where

$$\begin{aligned} \mathbf{N}(\boldsymbol{\nu}) &= \mathbf{C}(\boldsymbol{\nu}) + \mathbf{D}(\boldsymbol{\nu}) & \boldsymbol{h} &= [0,0,1]^\top \\ \boldsymbol{\alpha} &= [u_d, \alpha_2, -k_1 z_1 + r_d]^\top & z_1 &= \psi - \psi_d \\ \dot{\hat{\boldsymbol{b}}} &= \boldsymbol{\Gamma}\mathbf{R}(\psi)\boldsymbol{z}_2 & \boldsymbol{z}_2 &= \boldsymbol{\nu} - \boldsymbol{\alpha}\,. \end{aligned}$$

The variable α_2 is determined by a differential equation generated by the dynamic constraint $\tau_2 = Y = 0$. The constant parameter $k_1 > 0$ and matrix $\mathbf{K}_2 = \mathrm{diag}\{k_{21}, k_{22}, k_{23}\} > 0$ are tuning parameters of the controller. The constant matrix $\boldsymbol{\Gamma} > 0$ tunes the convergence rate of the estimator $\hat{\boldsymbol{b}}$, which estimates disturbances in the NED frame.

The reference signal for surge speed is $u_{\mathrm{ref}}(\theta(t))$, which is the planned surge speed at the path parameter $\theta(t)$ mentioned in Section 4. A reference model is used to generate smooth derivatives:

$$(u_d/u_{\mathrm{ref}})(s) = \omega_{n,u}^2/(s^2 + 2\zeta_u\omega_{n,u}s + \omega_{n,u}^2), \tag{8}$$

which is converted to a state-space representation, with saturation on the acceleration $\dot{u}_d(t)$.

The reference signal for heading is retrieved from the guidance controller: $\psi_{\mathrm{ref}} = \chi_d(t) - \beta(t)$, where $\beta(t)$ is the ship's sideslip angle $\beta(t) = \arcsin\frac{v(t)}{U(t)}$. The reference model in yaw is defined by the transfer function

$$\frac{\psi_d}{\psi_{\mathrm{ref}}}(s) = \frac{\omega_{n,\psi}^3}{(s + \omega_{n,\psi})(s^2 + 2\zeta_\psi\omega_{n,\psi}s + \omega_{n,\psi}^2)}, \tag{9}$$

which is converted to a state-space representation, with saturation on angular acceleration and velocity $\dot{r}_d(t)$ and $r_d(t)$.

4. PATH PLANNING BY PSEUDOSPECTRAL OPTIMAL CONTROL

PS methods may be used for solving the HJB equation, but for optimal control, a different approach is commonly used. The PS method discussed in this paper instead approximates the states and inputs as Lagrange polynomials, which are subsequently discretized. A discrete representation of the dynamics is applied as constraints, in addition to the equality and inequality constraints. The new optimization problem is then solved using a spectral algorithm (Gong et al., 2009).

Optimization-based complete path methods are based on the OCP:

Minimize

$$J(\boldsymbol{x}(\cdot), \boldsymbol{u}(\cdot), t_f) = E(\boldsymbol{x}(t_f), t_f) + \int_{t_0}^{t_f} F(\boldsymbol{x}(t), \boldsymbol{u}(t), t_f)\,\mathrm{d}t \tag{10a}$$

subject to

$$\dot{\boldsymbol{x}}(t) = \boldsymbol{f}(\boldsymbol{x}(t), \boldsymbol{u}(t), t) \tag{10b}$$
$$\boldsymbol{g}(\boldsymbol{x}(t), \boldsymbol{u}(t), t) \leq 0 \tag{10c}$$
$$\boldsymbol{h}(\boldsymbol{x}(t), \boldsymbol{u}(t), t) = 0 \tag{10d}$$
$$\boldsymbol{e}(\boldsymbol{x}(t_0), \boldsymbol{x}(t_f), t_0, t_f) = 0\,, \tag{10e}$$

where $\boldsymbol{x}(t)$ is the full state vector of the dynamic system, and $\boldsymbol{u}(t)$ is the control vector. The sense of optimality is defined in the cost function (10a), and the dynamics of the vehicle are included in the OCP as (10b). Path constraints (static obstacles), velocity and control constraints may be represented as (10c). Equality constraints may be included as (10d), and start and end conditions may be represented as (10e).

The cost function used in path planning is energy-based, and is defined as the work done by the actuators on the water:

$$J(\boldsymbol{x}, \boldsymbol{u}, t_f) = \int_{t_0}^{t_f} \left(|Xu_r| + |Yv_r| + |Nr|\right)\mathrm{d}t\,. \tag{11}$$

Since this energy function contains the non-smooth absolute value function, an approximation of this function is used for numerical efficiency: $|(\cdot)| = \sqrt{(\cdot)^2 + c}$, where $c > 0$ is a small constant, in our case $c = 0.001$.

The map where we perform path planning is defined by *path constraints*. For this we use elliptic shapes for virtual obstacles. Obstacle i is represented as

$$c_i(\boldsymbol{\eta}) = ((x - x_i)/x_{s,i})^2 + ((y - y_i)/y_{s,i})^2 \geq 1\,. \tag{12}$$

The center of the ellipse is x_i and y_i, and the latitudinal and longitudinal radii are $x_{s,i}$ and $y_{s,i}$. To avoid large numbers which may lead to numerical issues when the ship is far away from the obstacle, we take the logarithm of both sides of the inequality (12). The planning is in

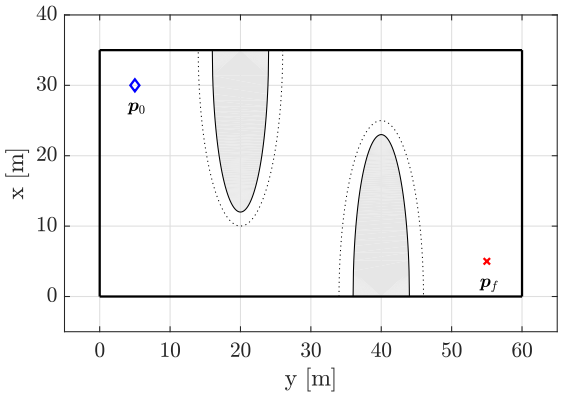

Fig. 5. Map used in path planning. The map shows virtual obstacles as dotted lines enclosing the actual obstacle with a safety margin.

this paper performed with two elliptic obstacles, with the parameters $x_1 = 35\,\text{m}$, $y_1 = 20\,\text{m}$, $x_{s,1} = 25\,\text{m}$, $y_{s,1} = 6\,\text{m}$; and $x_2 = 0\,\text{m}$, $y_2 = 40\,\text{m}$, $x_{s,2} = 25\,\text{m}$, $y_{s,2} = 6\,\text{m}$. These virtual obstacles should enclose actual obstacles in the map with a safety margin.

In addition to the elliptic obstacles, the search space is limited to the box $x \in [0, 35]\,\text{m}$, $y \in [0, 60]\,\text{m}$. This gives the map depicted in Fig. 5. The figure also shows the ship's start and goal locations as a blue diamond and red cross, respectively. Their positions are: $\boldsymbol{p}_0 = [30, 5]^\top\,\text{m}$ and $\boldsymbol{p}_f = [5, 55]^\top\,\text{m}$. The actuator values are limited to $F_{\min} \leq F(t) \leq F_{\max}$ where $F_{\min} = 0$ and $F_{\max} = 8\,\text{N}$, and $-\delta_{\max} \leq \delta(t) \leq \delta_{\max}$ where $\delta_{\max} = 30°$. The start time is $t_0 = 0$, and the final time t_f is limited to $0 \leq t_f \leq 150\,\text{s}$.

To generate a path with this method, the ship's pose $\boldsymbol{\eta}(t)$ and speed $\boldsymbol{\nu}(t)$ from (1) are changed to desired states, $\boldsymbol{\eta}_d(\theta)$ and $\boldsymbol{\nu}_d(\theta)$, respectively. Additionally, the time variable t in the OCP is changed to the path parameter θ. All related information retrieved from the planning will have the subscript $(\cdot)_d$, except for the planned course, which will be called the tangential course angle and have the notation $\chi_t(\theta)$, and the reference surge speed, which will have the notation $u_{\text{ref}}(\theta)$. The planning information used in simulation is the desired position $\boldsymbol{p}_d(\theta) = [x_d(\theta), y_d(\theta)]^\top$ and its derivative, the path-tangential angle $\chi_t(\theta)$ and the desired surge speed $u_{\text{ref}}(\theta)$.

The resulting OCP is solved using a software package for MATLAB: DIDO for PS optimal control by Elissar Global, on a computer with an Intel Core i7-7700HQ processor.

5. PLANNING AND SIMULATION RESULTS

Two different scenarios are explored in the results:

Scenario 1: (S1) Path planned using no current information.

Scenario 2: (S2) Path planned using correct current information.

After planning, both scenarios are simulated using a south-to-north current: $V_x = 0.1\,\text{m}\,\text{s}^{-1}$ and $V_y = 0$, equivalent to $0.84\,\text{m}\,\text{s}^{-1}$ for the full-scale ship. The ocean current

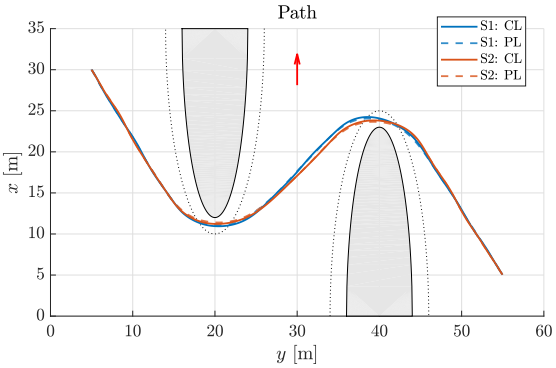

Fig. 6. Planned (PL) and closed-loop simulated (CL) paths from the two scenarios. The red arrow shows the resultant current direction.

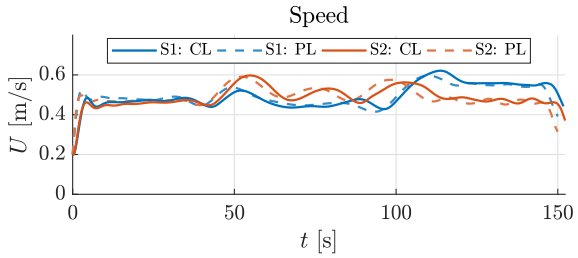

Fig. 7. Differences in speed between S1 and S2.

magnitude is a significant perturbation to the ship, and the direction is selected to be perpendicular to the main direction of travel. This is to demonstrate that using ocean current information in planning reduces the energy spent in transit. Closed-loop simulations are performed with the controllers detailed in Section 3. The results from planning are labeled PL, while the closed-loop simulation results are labeled CL.

The scenarios take place in the map shown in Fig. 5. The initial velocity is set to $\boldsymbol{\nu}_0 = [0.2, 0, 0]^\top\,\text{m}\,\text{s}^{-1}$ ($1.7\,\text{m}\,\text{s}^{-1}$ for the full-scale ship). The initial and final headings are free, but otherwise, the start and end conditions are set as mentioned in Section 4. The OCP solutions of S1 and S2 were found in 25 s and 21 s, respectively.

Figure 6 shows both the planned and simulated paths of S1 and S2. The planned paths are quite similar, however, especially when the ship maneuvers along the current direction, the path differs. This is also evident from Fig. 7, which shows significant speed differences between the scenarios after 50 s. These differences lead to significant changes in energy consumption between the two scenarios. An 8 % reduction of consumed energy is seen in Table 1, with the same time to completion t_f.

Table 1. Scenario results.

		Scenario 1		Scenario 2	
PL	J	124	J	153	J
CL	J	164	J	**151**	**J**
PL	t_f	150	s	150	s
CL	t_f	152	s	152	s

Figure 8 shows performance metrics for the two scenarios: On top is shown the cross-track error $e(t)$ from (4), while

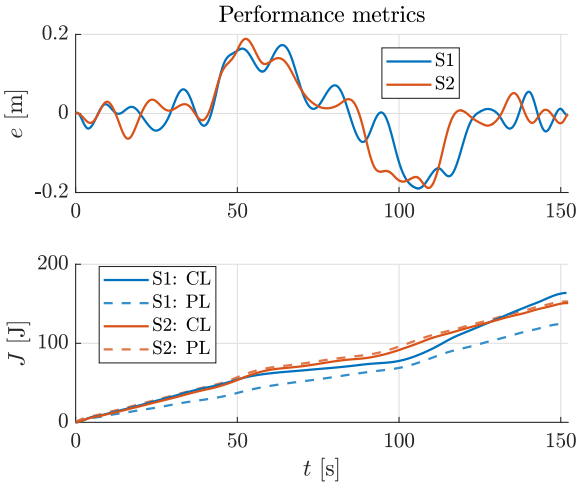

Fig. 8. Performance for both scenarios, both planned and simulated.

the accumulated energy consumption $J(t)$ from (11) is shown below. The cross-track error stays within 0.2 m for both scenarios, which is satisfactory and corresponds to 1.7 m for a full-scale ship. The simulated energy consumption in S1 surpasses the planned consumption, however, since this scenario is planned with no current information, the discrepancy is to be expected. In S2, the simulated energy consumption stays close to the planned consumption, and is significantly lower than in S1. An explanation to why the simulated consumption is slightly lower than planned may be that the integration method used in the PS algorithm differs from the simulation.

A notable observation from the resulting paths seen in Fig. 6 is that the planned (and the simulated) paths cross the obstacle boundaries. This is common with the PS method because the method only enforces constraints at the collocation points, of which there are only 30 in this case. One solution to avoid this is to increase the number of nodes at the expense of computational time, while another is to create the obstacle boundary with a safety margin outside the actual obstacle. The latter is preferable, because these are areas that are not desirable to enter.

6. CONCLUSIONS AND FUTURE WORK

A method for finding an energy-optimized path using pseudospectral optimal control has been proposed. Through closed-loop simulation with a guidance controller, this method has been verified to produce feasible and energy-efficient paths for a given underactuated 3-DOF ship model. Additionally, using up-to-date ocean current information helps to reduce energy spent. The method is suitable to use in combination with arbitrary curved-path guidance algorithms and low-level controllers. Several COLAV methods are also suitable to use with the path-planning method. Moreover, an overview of several path-planning methods is provided.

Exploring how the results from the PS path-planning method compares to other traditional roadmap planners is suggested for further work. Integrating the method with a complete COLAV system is also desirable, both in simulation and in real-world testing. Combining a COLAV system with regular re-planning might be necessary to retain optimality when the ship strays off course.

ACKNOWLEDGEMENTS

This work is funded by the Research Council of Norway and Innovation Norway with project number 269116. The work is also supported by the Centers of Excellence funding scheme with project number 223254.

REFERENCES

Bitar, G.I. (2017). *Towards the Development of Autonomous Ferries*. Master's thesis, NTNU.

Breivik, M. and Fossen, T.I. (2004). Path following for marine surface vessels. In *Proc. of the IEEE/MTS Oceans '04 Techno-Oceans Conf., Kobe, Japan*.

Criscione, V. (2017). Norway's greener future fleet. *Norway Exports*. URL `http://www.norwayexports.no/`.

DNV GL (2014). Sammenstilling av grunnlagsdata om dagens skipstrafikk og drivstofforbruk. Technical Report 2014-1667, Klima- og miljødepartementet.

Eriksen, B.O.H. and Breivik, M. (2017). MPC-based mid-level collision avoidance for ASVs using nonlinear programming. In *Proc. of the IEEE '17 CCTA, Mauna Lani, HI, USA*.

Fossen, T.I. (2011). *Handbook of Marine Craft Hydrodynamics and Motion Control*. Wiley-Blackwell.

Fredriksen, E. and Pettersen, K.Y. (2004). Global κ-exponential way-point manoeuvering of ships. In *Proc. of the 43rd IEEE CDC, Nassau, Bahamas*.

Gong, Q., Lewis, R., and Ross, I.M. (2009). Pseudospectral motion planning for autonomous vehicles. *Journal of Guidance, Control, and Dynamics*, 32(3), 1039–1045.

Kongsberg Maritime, Grenland Energy, NTNU, Fjellstrand, and Grønn Kontakt (2017). Lessons learned — best available technology. Technical Report 269116/E20, Pilot-E.

Lekkas, A.M., Roald, A.L., and Breivik, M. (2016). Online path planning for surface vehicles exposed to unknown ocean currents using pseudospectral optimal control. In *Proc. of the 10th IFAC CAMS, Trondheim, Norway*.

Rolls-Royce (2016). Rolls-Royce to supply first automatic crossing system to Norwegian ferry company Fjord1. *Rolls-Royce*. URL `https://www.rolls-royce.com/media/press-releases/yr-2016/18-10-2016-rr-to-supply-first-automatic-crossing-system-to-norwegian-ferry-company-fjord1.aspx`.

Ross, I.M. and Karpenko, M. (2012). A review of pseudospectral optimal control: From theory to flight. *Annual Reviews in Control*, 36(2), 182–197.

Skjetne, R., Fossen, T.I., and Kokotović, P.V. (2005). Adaptive maneuvering, with experiments, for a model ship in a marine control laboratory. *Automatica*, 41(2), 289–298.

Wilthil, E.F., Flåten, A.L., and Brekke, E.F. (2017). A target tracking system for ASV collision avoidance based on the PDAF. In *Sensing and Control for Autonomous Vehicles*. Springer International Publishing.

Wolek, A. and Woolsey, C.A. (2017). Model-based path planning. In *Sensing and Control for Autonomous Vehicles*. Springer International Publishing.